Generation and Characterization of Air Micro-bubbles in Highly Hydrophobic Capillaries

Charly Renard, Laurent Leclercq, Hervé Cottet

Generation and Characterization of Air Micro-bubbles in Highly Hydrophobic Capillaries

Charly Renard, Laurent Leclercq, and Hervé Cottet*

[1] IBMM, University of Montpellier, CNRS, ENSCM, France

*Correspondence should be addressed to the following author(s):

Prof. Hervé Cottet

IBMM, University of Montpellier, ENSCM, 34060 Montpellier, France

herve.cottet@umontpellier.fr

Keywords: Apparent charge / Electrophoretic mobility / Micro-bubbles generation / Superhydrophobic coatings

Abbreviations: BGE Background Electrolyte / CE Capillary Electrophoresis / DMF *N*,*N*-Dimethylformamide / GC Gas Chromatography / HEPES acide 4-(2-hydroxyéthyl)-1-pipérazine éthane sulfonique / I.D. Internal Diameter / NaOH Sodium hydroxyde

Abstract

The generation of air microbubbles in microfluidic systems or in capillaries could be of great interest for transportation (single cell analysis, organite transportation) or for liquid compartmentation. The physicochemical characterization of air bubbles and a better understanding of the process leading to bubble generation during electrophoresis is also interesting in a theoretical point of view. In this work, the generation of microbubbles on hydrophobic Glaco^{TM} coated capillaries has been studied in water-based electrolyte. Air bubbles were generated at the detection window and the required experimental parameters for microbubbles generation have been identified. Generated bubbles migrated against the electroosmotic flow, as would do strongly negatively charged solutes, under constant electric field. They have been characterized in terms of dimensions, electrophoretic mobility, and apparent charge.

1 Introduction

Gas bubbles are used for numerous applications: contrast agents for medical imagery by ultrasounds [1–3], therapeutic drug delivery by encapsulating the drug into the bubble [4–6], wastewater treatment [7], surface cleaning [7–9], froth flotation [10–12], drag reduction [9], sterilization of bacteria [13], enhanced germination rate of plant seeds [14], promotion of physiological activity of living organisms [15], and improved blood oxygenation [16]. Usually, air microbubbles are produced by mechanical agitation [17,18], or by increasing the temperature of cold (4°C) gas saturated water [19–21]. The presence of the nano or micro air bubbles in the liquid bulk can be observed using a laser beam via light scattering (Tyndall effect). The control of the air bubble size can be challenging but is still very important for the applications. The production of gas bubbles onto surfaces can be obtained by changing the solvent, for instance, by covering a surface with ethanol, and then slowly replacing the ethanol by water. The two liquids must be saturated with air or any other gas. Since ethanol has a higher gas solubility compared to water, a transient gas oversaturation occurs and the excess of gas results in the apparition of air bubbles onto the surface [22]. Another possibility to produce bubbles is to replace water with salted water, but the mechanism behind this phenomenon is not clear,

since air bubbles form when water is replaced by salted solution, but also when salted solution is replaced by water [23]. Another simple way to produce bubble onto a surface is by simply immersing the surface into water. When a dry surface is put in contact with a water droplet, there is an air pressure enhancement between the surface and the water droplet, leading to the formation of a dimple in the droplet, resulting in an air bubble [24]. This phenomenon is favored by the surface roughness/irregularities, as observed on superhydrophobic surfaces used in our study.

In capillary electrophoresis or in microfluidics in general, the presence of bubbles is usually not desired because it tends to destabilize the electrical current and to limit the repeatability of the separations [25]. It is therefore important to know in which conditions air bubbles can be formed and how to avoid them experimentally [25]. On the other hand, the generation of air microbubbles in microfluidic systems or in capillaries could be of great interest for transportation (single cell analysis, organites) [26,27] or for liquid compartmentation [28]. In this case, it is important, for practical reasons, to control the generation of the air bubbles [26]. The characterization of air bubbles, in terms of size, surface (or interface) charges, velocities or electrophoretic mobilities, is also crucial since these characteristics are leading their behavior and their fate in the environment in which they are formed/placed. The electrokinetic characteristics of air bubbles have been studied both theoretically [29,30], and experimentally [19,31,32]. Generally, negative zeta potentials were measured for air bubbles in water based electrolytes [19,31,32], except when cationic surfactant are present in the electrolyte leading to a reverse of the sign of the charge [19,32]. The origin of the negative charge is still under debates, but different explanations were proposed: an excess of hydroxide anions near the vapor/water surface [33,34]; Vacha et al. [35] and later Leroy et al. [30] suggested that the surface of the water molecules become partially charged due to a lack of balance between the number of donating and accepting hydrogen bonds. Zeta potential were derived from electrophoretic mobility measurements, generally performed by laser Doppler electrophoresis [19,32].

In a previous study [36], it was shown that Glaco^{TM} coated capillaries led to superhydrophobic capillaries (with meniscus inversion compared to fused silica capillary and slipping conditions at the capillary surface). The existence of a

nanometric air layer at the interface between the coating and the aqueous phase in the Glaco™ capillaries was proved by ellipsometry [36] and was also put in evidence by the 'mirror' effect observed on a Glaco™ coated blade immersed in water. These superhydrophobic capillaries were obtained by the deposition of a 1 µm thickness film of Glaco™ solution (containing nanostructured hydrophobically modified silica nanoparticles) by flushing the 50 µm I.D. × 40 cm capillary previously filled with the Glaco™ solution with air at a constant pressure of 100 psi [36]. The film of Glaco™ solution was next dried in a GC-oven. However, the resulting superhydrophobic capillaries were hardly filled with water-based electrolyte, leading to a 'train' of air bubbles in the capillary and to unstable current intensity in CE [36]. Stable current intensities were only obtained after a few electrophoretic runs, when the superhydrophobicity was reduced.

In this work, the use of 80 psi instead of 100 psi to flush the capillary previously filled with the Glaco™ solution during the coating protocol leads to slightly thinner Glaco™ liquid film deposition (0.9 µm) onto the capillary surface, and thus to slightly lower superhydrophobicity. The 80 psi-Glaco™ coated capillaries can be easily filled with water-based electrolyte and lead to stable current intensity in CE. The generation of air bubbles inside such capillary has been studied in water based electrolyte. Air bubbles were generated at the detection window and the required parameters for micro-bubbles generation have been identified. Generated bubbles were displaced by electrophoretic migration under constant electric field and have been characterized in terms of dimensions, electrophoretic mobility, and apparent charge.

2 Materials and methods

2.1 Chemicals

Glaco Mirror Coat Zero™ was purchased from Soft99 (Osaka, Japan). It is composed of silica nanoparticles suspension (hydrophobically modified with alkyl groups) dispersed in isopropanol. The nanoparticle concentration in the Glaco™ solution is about 4 $g.L^{-1}$, as quantified by weighing the dry residue after evaporation of the solvent. Ultrapure grade water (18 $M\Omega.cm^{-1}$) was produced on a Milli-Q

equipment (Merck Millipore, USA). Sodium hydroxide (NaOH) and *N*,*N*-dimethylformamide (DMF, 99%) were purchased from Sigma-Aldrich (St Quentin Fallavier, France). 4-(2-hydroxyethyl)-1-piperazine ethanesulfonic acid (HEPES) was purchased from VWR (Fontenay-sous-bois, France). Brilliant Blue FCF (food coloring, E133) from Vahiné (Avignon, France) was used as an aqueous colorant. Mesityl Oxide (4-metyl-4-penten-2-one) was purchased from Alfa Aesar (Thermo Fischer Scientific, Karlsruhe, Germany).

2.2 Glaco™ coated capillaries

Glaco Fused silica capillaries (PolyMicro Technologies, Photonlines, Saint-Germain-en-Laye, France) of 360 µm external diameter, 50, 100 or 180 µm internal diameter (I.D.) × 40 cm total length (30 cm to the detector window) were coated with Glaco™ by flushing the capillary with the Glaco™ suspension. Excess of Glaco™ solution was then removed by flushing the capillary with air to obtain a 0.9 µm liquid film on the capillary wall, as given by equation (1) [37]:

$$\varepsilon = 1.34\, R_c^{7/3} \left(\frac{\Delta P}{8 L \gamma} \right)^{2/3} \quad (1)$$

where ε is the thickness of the deposited film, R_c is the inner radius of the capillary, ΔP is the applied air pressure, L is the total capillary length and γ is the surface tension of the Glaco™ solution (20 $N.m^{-1}$). Equation (1) was obtained by combining the Poiseuille with the Landau, Levich and Derjaguin (LLD) theory [37] giving:

$$\varepsilon = 1.34\, R_c Ca^{2/3} \quad (2)$$

where *Ca* is the dimensionless capillary number defined by equation (3):

$$Ca = \frac{\eta V}{\gamma} \quad (3)$$

where V is the linear velocity of the coating solution flushed by air pressure (in $m.s^{-1}$). The experimental conditions for the flushing pressures and times are displayed in Table 1 according to the capillary I.D. Glaco™ coatings were then thermally stabilized by placing the capillaries in a GC-2010 Plus oven (Shimadzu, Marne-la-Vallée, France) for 15 min at 250°C without any gas flow. The same process

(Glaco™ deposition and thermal stabilization) was repeated 3 times. Capillaries were finally left overnight under ambient air at room temperature before use.

Table 1. Coating protocol for the preparation of Glaco™ coated capillaries (Fused silica capillaries of 40 cm × 360 µm O.D. × I.D. as indicated in the Table). The entire protocol is repeated 4 times by alternating the flushing direction in the capillary (alternatively from the starting or the ending ends of the capillary).

Capillary I.D.	50 µm	100 µm	180 µm
Glaco™ flushing	20 psi, 5 min	5 psi, 5 min	1.5 psi 5 min
Air flushing	80 psi, 5 min	20 psi, 5 min	6.2 psi 5 min

2.3 Capillary electrophoresis

Capillary electrophoresis experiments were carried out on a P/ACE™ MDQ Beckman-Coulter (Sciex, Villebon sur Yvette, France) piloted by 32 Karat software. Glaco™ coated capillaries of 50 µm internal diameter (I.D.), 40 cm total length (30 cm to the detector window), were coated as described in section 2.2 and used for air bubble generation. Unless otherwise specified, all electrolytes were prepared with boiled ultrapure water to obtain gas-free solutions. The degassing step appeared to be primordial in previous studies [36] as it allowed for stable current during the whole runs. Without degassing, the gasses dissolved into the aqueous phase interacted with the capillary air layer to form bubbles obstructing the flow and thus breaking the conductivity of the background electrolyte. Electrophoretic migrations were performed in a 20 mM HEPES + 10 mM NaOH background electrolyte at pH 7.4 (10 mM ionic strength). Capillaries were flushed at 20 psi for 3 min with the background electrolyte before each run. DMF (at the concentration of 1 % in the electrolyte) was used as an electroosmotic flow marker. Electrophoretic migrations were realized using +20 kV voltage (unless otherwise specified) and +3 psi pressure at both capillary ends to stabilize the electrical current.

3 Results and discussion

Inadvertently and surprisingly, we have noticed that microbubbles could be easily generated in a controlled manner in 80 psi-Glaco™ coated capillaries. We have also noticed that these bubbles can move into the capillary and migrate under electric field. The aim of this study is to identify the conditions of appearance of these bubbles and to characterize these bubbles in terms of charge, electrophoretic mobility and size.

3.1 Highlighting the generation of air bubbles during electrophoresis on a Glaco™ coated capillary

Figure 1 shows the meniscus of a blue colored-water plug in a Glaco™ coated capillaries of different diameters (50, 100 and 180 µm, respectively), according to the coating protocol detailed in section II.2 (with a deposition thickness of Glaco™ solution of about 0.9 µm). The meniscus shape is reversed compared to fused silica capillary with a contact angle of about α=120°, which proves that the coating is highly hydrophobic but significantly lower than for a 1 µm film deposition (α=159°) [36].

Figure 2 displays the current intensity (in green) and the UV trace (in blue) obtained in the Glaco™ coated capillary under +20 kV voltage in a 20 mM HEPES/Na buffer pH 7.4, when the inlet vial contains 1% DMF solution (used as EOF marker in frontal continuous electrophoresis mode) in the BGE. The increase of the UV trace corresponds to the detection of the DMF reaching the detection window. Surprisingly, a few seconds later, UV spikes appeared regularly with simultaneous fall of the current intensity. Spikes combined with current intensity drop can be explained by the formation of air bubbles generated at the detection point. The air bubble passing in front of the detection point modified the absorbance signal, generating a spike, and the presence of low-conductivity zone in the BGE decreased the current intensity. It is worth noting that these experiments were reproducible, as demonstrated by Figure SI1 showing similar results in the same electrophoretic conditions but on a different Glaco™ coated capillary according the same coating protocol.

There are several experimental parameters that are required to generate the air bubbles. They are listed hereafter: (*i*) the 80 psi Glaco™ coated capillary is required; (*ii*) the UV lamp should be turned on since the electrical current intensity was not affected when the same experiment as in Figure 2 was conducted in absence of UV radiation; (*iii*) the separation voltage is also required and no bubble was observed under hydrodynamic flow without separation voltage; (*iv*) a DMF concentration of at least 0.5% is required (lower DMF concentrations or the use of other marker such as mesityl oxide did not generate bubbles, see Figure SI2).

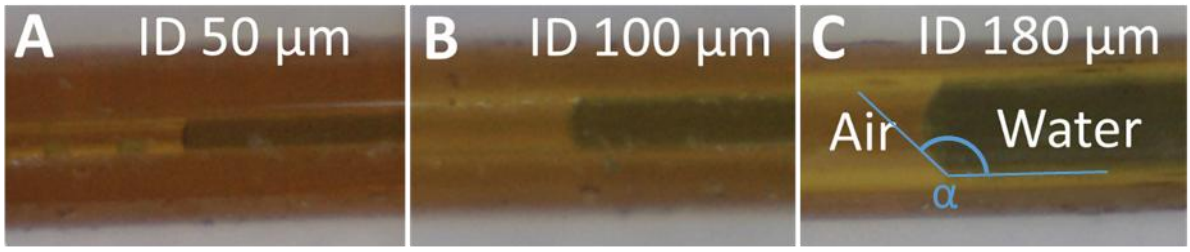

Figure 1. Visualization of the meniscus in Glaco™ coated capillaries of different internal diameters **(A**: 50 µm ID ; **B**: 100 µm ; **C**: 180 µm) by optical microscopy (magnification ×50). Capillaries are filled with blue colored water (dyed with E133 at 1 $g.L^{-1}$) and with air to see the interface. Glaco™ coated capillaries were prepared according to the protocol given in section II.2. α is the contact angle (~120 °).

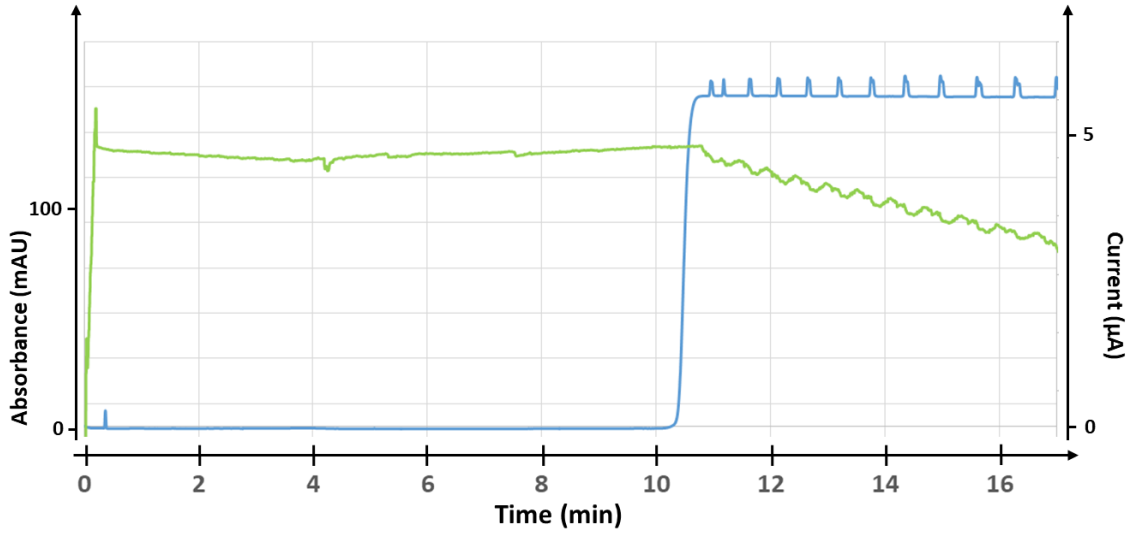

Figure 2. Electropherogram (blue trace) of 1% DMF marker in frontal mode obtained on Glaco™ coated capillary showing the generation of air bubbles. The corresponding current intensity is displayed in green. Experimental conditions: Glaco™ coated capillary 50 µm I.D. × 40 cm length (30 cm to the detector) prepared according to section 2.2. Background electrolyte: 20 mM HEPES + 10 mM NaOH at

pH 7.4. Applied voltage: +20 kV. Pressure (to stabilize the current intensity): + 3 psi at both capillary ends. Inlet vial: DMF at 1% in BGE. Outlet vial: BGE. Capillary flush with BGE before the run: 20 psi, 3 min. Detection: 214 nm. Temperature: 25°C.

3.2 Electrophoretic mobility and zeta potential of air bubbles

Air bubble electrophoretic apparent velocity and dimensions can be both determined (or estimated) from the experiment described in Figure 3. Frontal continuous electrophoresis of 1% DMF in BGE was performed as in Figure 2 (see Figure 3, step 1); however the voltage was rapidly stopped once a bubble was detected. Then, a mobilization pressure was applied in order to detect a second time the bubble in front of the detector (see Figure 3, step 3). The direction of the hydrodynamic flow to apply to detect the bubble a second time was identified on a trial and error principle, since it depends on the direction of the apparent velocity of the bubble during the electrophoretic process. It was found that the apparent electrophoretic velocity of the air bubble was against the electroosmotic flow (toward the inlet side of the capillary, as for a highly charged anion). Just before the mobilization pressure, the inlet vial was replaced by a 1.5% DMF in BGE (step 3) in order to be able to determine the mobilization pressure velocity.

In order to determine the apparent and effective electrophoretic mobility of the air bubble in the capillary during the electrophoretic process, it was assumed that the air bubble moved at the same velocity ($v_{hydro,bubble}$) that the velocity of the DMF front ($v_{hydro,DMF}$) during the mobilization pressure step (step 3 in Figure 3), leading to equation (4):

$$v_{hydro,DMF} = \frac{l}{t_{hydro,DMF}} = v_{hydro,bubble} = \frac{d_{hydro,bubble}}{t_{hydro,bubble}} \quad (4)$$

where l is the effective capillary length, $t_{hydro,DMF}$ is the migration time of the 1.5% DMF front to reach the detection window under 3 psi pressure (2.78 min) during the mobilization pressure step, $d_{hydro,bubble}$ is the distance between the air bubble and the detection point just before applying the mobilizing pressure, and $t_{hydro,bubble}$ is the time taken by the air bubble to reach the detection window once the pressure was applied (0.36 min). From equation (4), it is possible to determine $v_{hydro,bubble} = 1.8\times10^{-3}$ m.s^{-1} and $d_{hydro,bubble}$=38.8 mm. Assuming that $d_{hydro,bubble}$ is equal to the distance $d_{electro,bubble}$ travelled by the bubble from the detection point during the electrophoretic

process after the bubble formation, one can determine the apparent electrophoretic velocity $v_{electro,bubble}$ of the air bubble during the electrophoretic migration by:

$$v_{electro,bubble} = \frac{d_{hydro,bubble}}{t_{electro,bubble}} \quad (5)$$

where $t_{electro,bubble}$ is the time between the air bubble first apparition at the detection window and the electrical field stop (0.34 min). From eq. (5), we get $v_{electro,bubble}$=1.9×10^{-3} m.s^{-1} corresponding to an apparent electrophoretic mobility of μ_{app} = -38.0×10^{-9} m²V^{-1}s^{-1}. Knowing that the electroosmotic mobility μ_{eo} = +10.9×10^{-9} m²V^{-1}s^{-1} from the DMF migration time, the effective electrophoretic mobility of the air bubble was determined as: $\mu_{ep} = \mu_{app} - \mu_{eo}$= -48.9×10^{-9} m²V^{-1}s^{-1}. The air bubbles bear therefore strongly negative charges on their surfaces, which correspond to a zeta potential of about ~ -62.6 mV, assuming that the air bubble behaves according to the Smoluchowski law:

$$\zeta = \frac{\mu_{ep}\eta}{\varepsilon_0\varepsilon_r} \quad (6)$$

where ε_0 is the vacuum permittivity (8.85×10^{-12} F·m^{-1}), ε_r is the water relative permittivity (ε_r=78), and η is the electrolyte viscosity (0.89 cP). The validity of the Smoluchowski law is verified since ξ< 100 mV and κR_h > 100, where κ is the reciprocal of the Debye length (κ^{-1} ~ 3 nm) and R_h is the characteristic size of the solute (air bubble in this study, ~ 40 µm × 10 mm, see section 3.3).

The origin of the negative charges at the liquid/gas interface can be attributed to the adsorption phenomena of OH^- anions on the bubble surface [33,34], which was also observed on solid nanoparticles [18]. This theory is supported by the fact that the bubbles were much more stable (i.e. the electrostatic force was higher) in alkaline water solution than in a neutral or acidic one. Some authors also considered the increased autolysis of water molecules to explain higher hydroxyde content at the surface [34]. But this general interpretation is still under debate, and other authors developed, more recently, a surface complexation model based on the presence of negative surface sites due to the fact that the balance of accepting and donating hydrogen bonds is broken at the interface [30,35]. Regarding the origin of the air/gas inside the bubble that we observed, since the BGE was degassed, a possibility could

be that some of the air trapped at the highly hydrophobic capillary surface is destabilized and expulsed in the bubbles.

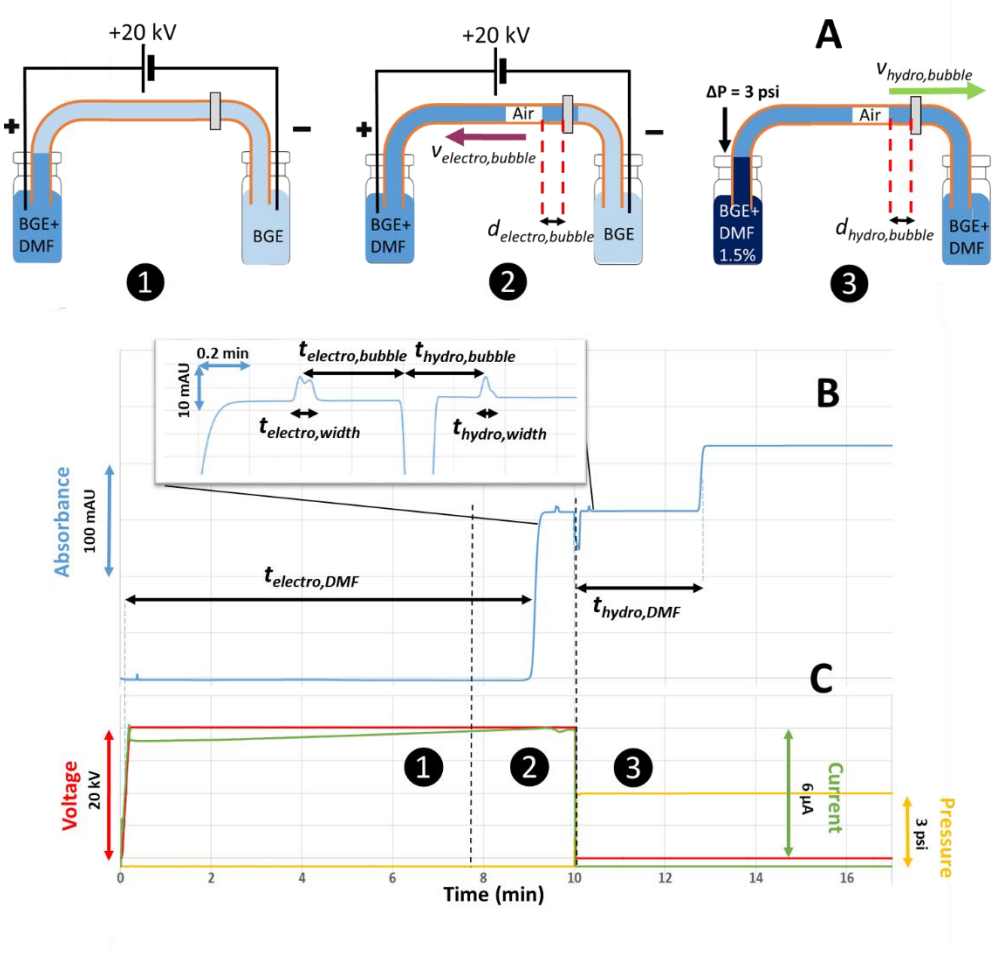

Figure 3. Details of the experimental sequence implemented to determine the dimensions and electrophoretic mobility of an air bubble generated during the electrophoresis of a DMF front in a 80 psi-Glaco™ coated capillary. Schematic representation of the DMF front and the air bubble positions in the capillary at different times (A), of the UV trace at 200 nm (B) and the corresponding voltage (in red) / pressure (in yellow) / current intensity (in green) sequence (C). Experimental conditions: Glaco™ coated capillary, 50 µm × 40 cm length (30 cm to the detector). Background electrolyte: 20 mM HEPES + 10 mM NaOH at pH 7.4. At *t*=0, BGE was in the capillary and in the outlet vial, while the inlet vial contained BGE + DMF. Separation voltage: +20 kV from 0 to 10 min. The 1% DMF front reached the detection window at 9.1 min under electrophoretic process and generated one air bubble detected at 9.7 min. The air bubble then migrated towards the inlet end of the capillary until voltage was suppressed. From *t*= 10 min, the voltage was stopped, the inlet vial was replaced by a vial containing 1.5% DMF in BGE and a + 3 psi mobilization pressure was applied. At 10.4 min, the air bubble reached the detection window, followed by the 1.5 % DMF front which reaches the detector at 12.8 min. Flush before experiment: 20 psi, 3 min with BGE. Steps 1 to 3 are commented in the text.

3.3 Air bubble dimensions

The dimensions of the air bubble can change under the influence of an electric field [38]. Knowing the apparent air bubble velocities both under electrical field $v_{electro,bubble}$ (equation 5) and under pressure $v_{hydro,bubble}$ (equation 4), it was thus possible to calculate the air bubble length (or width) by measuring the time the air bubble took to cross the detection window (i.e. the temporal air bubble width measured as $t_{electro,width}$ = 0.092 min under electrical field and $t_{hydro,width}$ = 0.067 min under pressure mobilization), using equations (7) and (8):

$$l_{electro,bubble} = v_{electro,bubble}\ t_{electro,width} \quad (7)$$

$$l_{hydro,bubble} = v_{hydro,bubble}\ t_{hydro,width} \quad (8)$$

Those equations lead to $l_{electro,bubble}$ = 10.5 mm and $l_{hydro,bubble}$ = 7.24 mm, illustrating the difference in size of a given air bubble with and without applied voltage, respectively. This is also in good agreement with the fact that the air bubble tends to spread under the influence of an electric field [38].

The presence of air bubbles in the capillary lowers the global conductivity of the capillary, since the air bubble are non-conductive. This explains why the current intensity is progressively decreasing with the generation of the air bubbles in the capillary. Since the current intensity is not completely shut down but just decreased, it can be considered that the air bubbles are not clogging all the capillary section (see Figure 4). The overall resistivity R of the capillary is the sum of the individual resistivity pertaining to each bubble and the resistivity of the portions of capillary with no air bubble. As a first approximation, we consider in this model that all the air bubbles have the same given length $l_{electro,bubble}$. Therefore, in an electrical point of view, the overall resistivity of the capillary of length L can be obtained by considering the resistivity R_{bubble} due to the n bubbles which occupy a length L_1, and the resistivity of the BGE on a capillary length (L-L_1), as illustrated in Figure 4. R_{bubble} can be expressed as a function of L_1, the conductive section S_1 in the air bubble zone, and the BGE conductivity κ according to:

$$R_{bubble} = \frac{L_1}{\kappa S_1} \quad (9)$$

Similarly, the resistivity of the portion of capillary without air bubble is given by:

$$R_{no\,bubble} = \frac{L - L_1}{\kappa S} \quad (10)$$

where S is the conductive section of the capillary without bubble and L the total capillary length. The conductivity of the 20 mM HEPES/Na BGE is κ = 6.3 10^{-2} $\Omega^{-1}m^{-1}$ as calculated from the current intensity obtained in similar electrophoretic conditions in a 50 µm I.D. × 40 cm bare fused silica capillary (i.e. without any air inside the capillary). In order to determine the air bubble diameter d_{air}, the Ohm law is expressed using equations (9) and (10) by:

$$V = RI = \left(\frac{L - L_1}{\kappa S} + \frac{L_1}{\kappa S_1} \right) I \quad (11)$$

Replacing L_1 by $n_{bubble} \times l_{electro,bubble}$ in equation (11) leads to equation (12) where 1/I is expressed by:

$$\frac{1}{I} = \left(\frac{L - n_{bubble} l_{electro,bubble}}{S} + \frac{n_{bubble} l_{electro,bubble}}{S_1} \right) \frac{1}{\kappa V} \quad (12)$$

with $n_{bubbles}$ being the number of bubbles present in the capillary at a given migration time. Deriving equation (12) according to the migration time, leads to equations (13):

$$\frac{d}{dt}\left(\frac{1}{I}\right) = \frac{dn_{bubble}}{dt} \frac{l_{electro,bubble}}{\kappa V} \left(\frac{1}{S_1} - \frac{1}{S} \right) \quad (13)$$

where $d(1/I)/dt$ = 232.7 $A^{-1}s^{-1}$ is the slope of the dotted trace in Figure 5 and dn_{bubble}/dt = 0.0305 s^{-1} is the slope of the orange trace in Figure 5. Equation (13) can be used to determine S_1 according to:

$$S_1 = \frac{1}{\frac{\kappa V}{l_{electro,bubble}} \frac{\frac{d}{dt}\left(\frac{1}{I}\right)}{\frac{dn_{bubble}}{dt}} + \frac{1}{S}} \quad (14)$$

Taking $l_{electro,bubble}$ = 13 mm in equation (14) leads to S_1= 7.99 10^{-10} m^2. d_{air} was then determined using equation (15), with S_1 obtained from equation (14), giving d_{air} of 37 µm:

$$d_{air} = \sqrt{\frac{4(S - S_1)}{\pi}} \quad (15)$$

Therefore, we can estimate the bubble diameter to ~ 37 µm. The experimental method leading to equations (14) and (15) has the advantage to average the experimental data on 11 bubbles created in a period of time corresponding to about 5-6 min (see Figure 5).

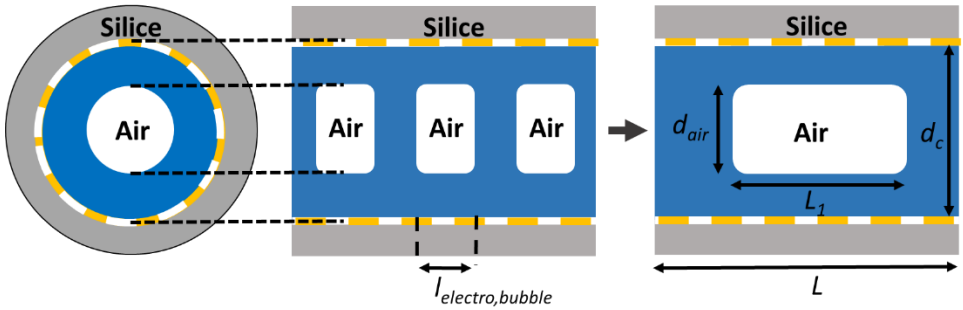

Figure 4. Schematic representation of the air bubble repartition in a Glaco™ coated capillary for the modelling of the overall capillary resistivity *R*. The air bubbles are considered as a succession of identical zones having a length $l_{electro,bubble}$ under electric voltage. In an electrical point of view, the capillary resistivity can be viewed as the sum of two contributions: an air portion of capillary length L_1 with a diameter d_{air} gathering all the air bubbles and a portion of capillary L-L_1 only filled with BGE of diameter d_c. S_1 is the section of capillary occupied by the BGE in presence of an air bubble and *S* is the section of capillary occupied by the BGE in absence of air bubble.

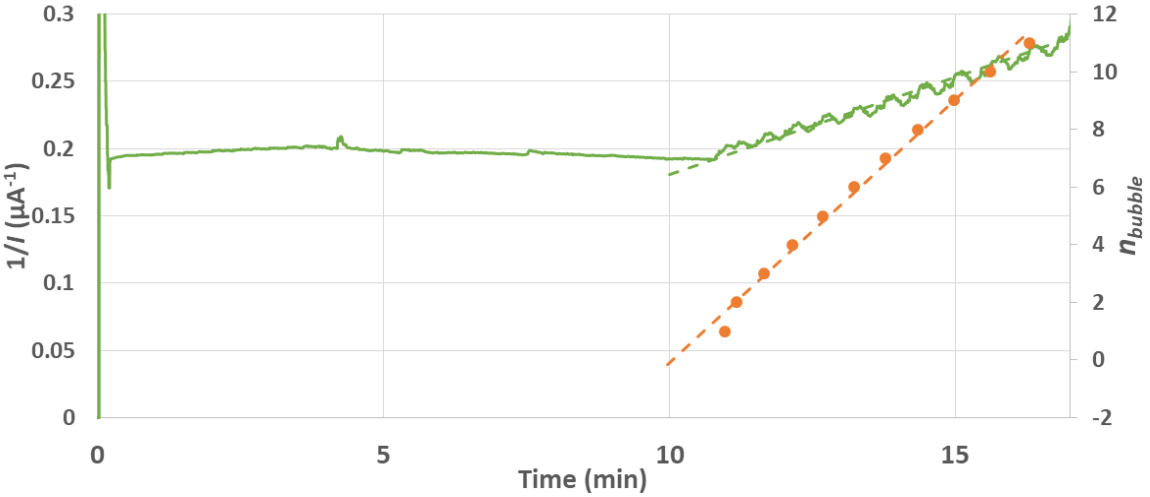

Figure 5. Representation of the inverse of the current intensity evolution (green trace) during DMF marker migration in a 80 psi-Glaco™ coated capillary and the corresponding number of generated bubbles (in orange). Starting at around 11 min, each current intensity perturbation increment is related to the formation of one air bubble (also identified by an orange dot). The global decreasing current intensity slope is d(1/*I*)/dt= 232.7 $A^{-1}s^{-1}$. The slope dn_{bubble}/dt = 1.83 bubble min^{-1} = 0.0305

bubble s^{-1} (slope of the dotted orange line). Experimental conditions and experimental data as in Figure 2.

3.4 Influence of the applied separation voltage on the bubble formation and characteristics

DMF migration similar to the experiment of Figure 2 was performed at 4 different voltages (30 kV, 20 kV, 15 kV and 10 kV) as displayed in Figure 6 showing the corresponding UV traces and current intensities. The bubble characteristics ($l_{electro,bubble}$, d_{air}, bubble frequency, distance between bubbles) and the electrophoretic figures of merit (EOF mobility, electrophoretic velocity of the bubble) have been studied. The measurements were made on at least 6 successive bubbles on each run, and the results are summarized in Table 2. Calculations were done following the same approach as used in section 3.3. As expected, modifying the separation voltage allowed decreasing the apparent electrophoretic velocity value from 2.95 $mm.s^{-1}$ at 30 kV down to 0.94 $mm.s^{-1}$ at 10 kV. It is thus possible to modulate the migration velocity of the bubbles, by simply changing the applied voltage. Regarding the dimensions of the bubbles, the diameter of the bubble was relatively constant (about d_{air} ~36-41 µm), whatever the applied voltage. The bubble length under electric field was about $l_{electro,bubble}$~8-9 mm, except at 10 kV for which the length was about 2 times lower (~4.4 mm). The frequency of the bubbles was comprised between 0.053 Hz and 0.035 Hz.

μ_{eo} was roughly the same at each applied voltage, as expected. Hence, $v_{electro,bubble}$ was directly proportional to the applied voltage. The distance between two bubbles is the same at 30 kV and 20 kV (about 5 cm), and decreased to about 2 to 3 cm at 10 kV and 15 kV, respectively. On the whole, better stability and regularity in the bubble formation was observed at 30 kV and 20 kV compared to 15 and 10 kV.

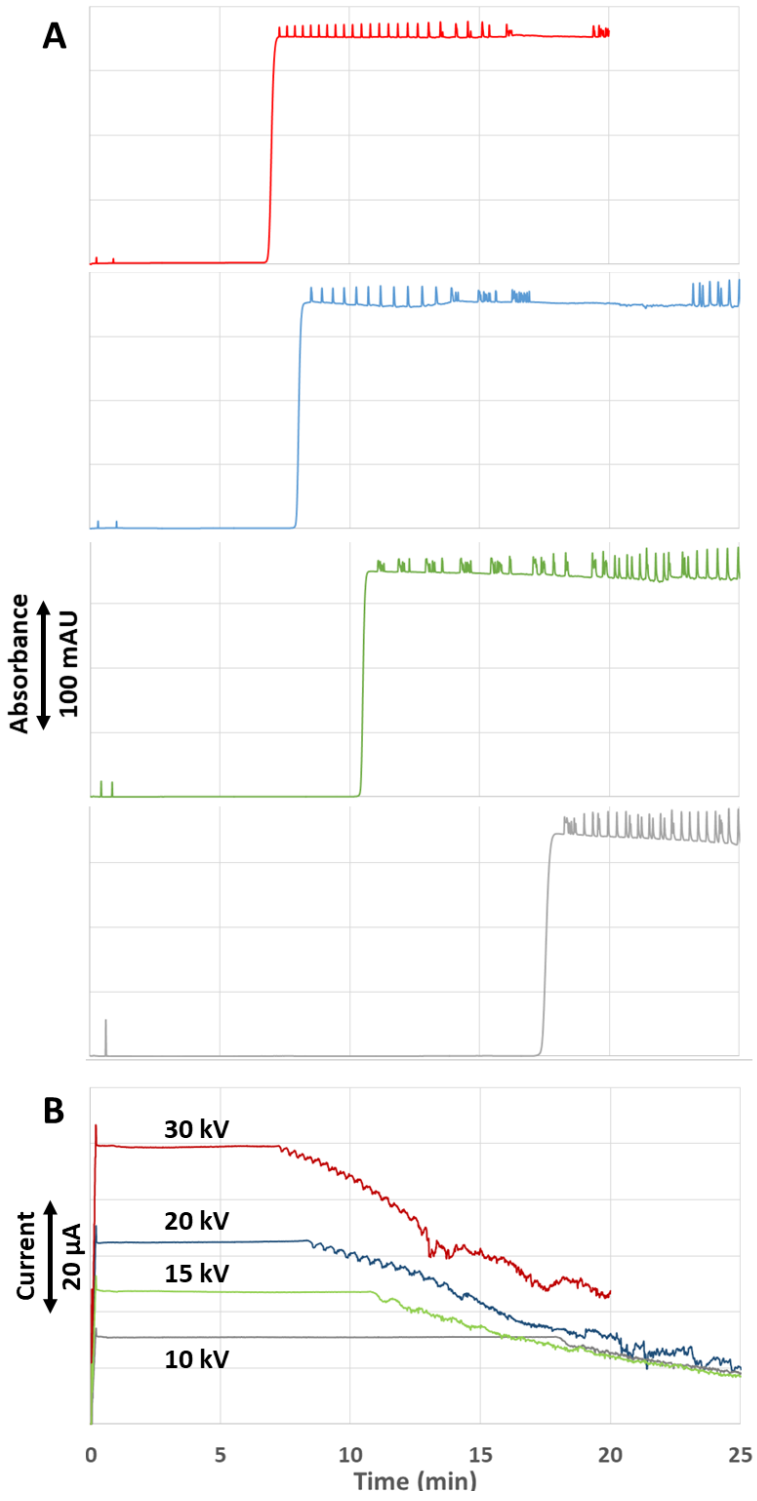

Figure 6: Electropherograms of 1% DMF marker in frontal mode obtained on 80 psi-Glaco™ coated capillary showing the generation of air bubbles at 30 kV (light red), 20 kV (light blue), light green (15 kV) and 10 kV (light grey) (A) and the corresponding current intensities (same color but darker) (B). Experimental conditions: Glaco™ coated capillary 50 µm I.D. × 40 cm length (30 cm to the detector) prepared according to section II.2. Background electrolyte: 20 mM HEPES + 10 mM NaOH at pH 7.4. Pressure (to stabilize the current intensity): + 3 psi at both capillary ends. Inlet vial: DMF at 1% in BGE. Outlet vial: BGE. Capillary flush with BGE before the run: 20 psi, 3 min. Detection: 214 nm. Temperature: 25°C.

Table 2. Bubble characteristics at three different applied voltages. Experimental conditions as in Figure 6. Electrophoretic mobility of the bubble: μ_{ep} = -48.9×10^{-9} m²V^{-1}s^{-1}.

Voltage (kV)	30	20	15	10
μ_{eo} (10^{-9} m² V^{-1}s^{-1})	9.5	12.4	12.7	11.4
μ_{app} (10^{-9} m² V^{-1}s^{-1})	-39.4	-36.4	-36.2	-37.5
$v_{electro,bubble}$ (mm.s^{-1})	2.95	1.82	1.36	0.94
$l_{electro,bubble}$ (mm)[a]	8.7	9.3	8.5	4.6
Bubble frequency (s^{-1})	0.0527	0.0345	0.0401	0.0516
d_{air} (µm)	35.8	35.9	41.2	39.0
Distance between bubbles (mm)	55.9	52.7	33.8	18.2

[a)] mean value of the first 11 bubble lengths of each run for the runs at 30 and 20 kV, and mean value of the 6 more stable bubbles for the run at 15 kV (the six consecutive bubbles between 24 and 26 min) and 10 kV (the six consecutive bubbles between 19 and 21 min).

4 Concluding remarks

This work demonstrates that it is possible to repeatedly generate air microbubbles at the detection window of an hydrophobic Glaco^{TM} coated capillary. In addition to the specific capillary coating, several experimental requirements have been identified: (*i*) the UV lamp should be turned on; (*ii*) the separation voltage is also mandatory; (*iii*) a DMF concentration of at least 0.5% is required in front of the detection window to generate the bubbles. Air microbubbles have a diameter of about d_{air} ~35-39 µm, a typical length of about 10 mm and an effective electrophoretic mobility of about -48.9×10^{-9} m²V^{-1}s^{-1}. The air bubbles bear therefore strongly negative charges on their surfaces corresponding to a zeta potential of about ~ -62.6 mV. As expected, modifying the separation voltage allows changing the apparent electrophoretic velocity from 2.95 mm.s^{-1} at 30 kV down to 0.94 mm.s^{-1} at 10 kV. This approach could be useful to generate on demand air microbubbles, for instance by controlling the zones of DMF in the capillary, or by controlling the switching on/off of the UV beam during the run.

Conflict of interest

The authors have declared no conflict of interest.

Data Availability Statement

The data that support the findings of this study are available from the corresponding author upon reasonable request.

5 References

[1] Hettiarachchi, K., *Lab Chip* 2001, *7*, 1–37.

[2] Tian, J., Yang, F., Cui, H., Zhou, Y., Ruan, X., Gu, N., *ACS Appl. Mater. Interfaces* 2015, *7*, 26579–26584.

[3] Yin, T., Wang, P., Zheng, R., Zheng, B., Cheng, D., Zhang, X., Shuai, X., *Int. J. Nanomedicine* 2012, *7*, 895–904.

[4] Wang, Y., Li, X., Zhou, Y., Huang, P., Xu, Y., *Int. J. Pharm.* 2010, *384*, 148–153.

[5] Misra, S.K., Ghoshal, G., Gartia, M.R., Wu, Z., De, A.K., Ye, M., Bromfield, C.R., Williams, E.M., Singh, K., Tangella, K.V., Rund, L., Schulten, K., Schook, L.B., Ray, P.S., Burdette, E.C., Pan, D., *ACS Nano* 2015, *9*, 10695–10718.

[6] Meng, M., Gao, J., Wu, C., Zhou, X., Zang, X., Lin, X., Liu, H., Wang, C., Su, H., Liu, K., Wang, Y., Xue, X., Wu, J., *Tumor Biol.* 2016, *37*, 8673–8680.

[7] Agarwal, A., Ng, W.J., Liu, Y., *Chemosphere* 2011, *84*, 1175–1180.

[8] Zhu, J., An, H., Alheshibri, M., Liu, L., Terpstra, P.M.J., Liu, G., Craig, V.S.J., *Langmuir* 2016, *32*, 11203–11211.

[9] Ushida, A., Hasegawa, T., Takahashi, N., Nakajima, T., Murao, S., Narumi, T., Uchiyama, H., *J. Surfactants Deterg.* 2012, *15*, 695–702.

[10] Calgaroto, S., Wilberg, K.Q., Rubio, J., *Miner. Eng.* 2014, *60*, 33–40.

[11] Fan, M., Tao, D., Honaker, R., Luo, Z., *Min. Sci. Technol.* 2010, *20*, 159–177.

[12] Sobhy, A., Tao, D., *Int. J. Miner. Process.* 2013, *124*, 109–116.

[13] Kawara, F., Inoue, J., Takenaka, M., Hoshi, N., Masuda, A., Nishiumi, S.,

Kutsumi, H., Azuma, T., Ohdaira, T., *Digestion* 2014, *90*, 10–17.

[14] Liu, S., Oshita, S., Makino, Y., Wang, Q., Kawagoe, Y., Uchida, T., *ACS Sustain. Chem. Eng.* 2016, *4*, 1347–1353.

[15] Liu, S., Kawagoe, Y., Makino, Y., Oshita, S., *Chem. Eng. Sci.* 2013, *93*, 250–256.

[16] Matsuki, N., Ishikawa, T., Ichiba, S., Shiba, N., Ujike, Y., Yamaguchi, T., *Int. J. Nanomed.* 2014, *9*, 4495–4505.

[17] Ferrara, K.W., Borden, M.A., Zhang, H., *Acc. Chem. Res.* 2009, *42*, 881–892.

[18] Nirmalkar, N., Pacek, A.W., Barigou, M., *Langmuir* 2018, *34*, 10964-10973.

[19] Najafi, A.S., Drelich, J., Yeung, A., Xu, Z., Masliyah, J., *J. Colloid Interface Sci.* 2007, *308*, 344–350.

[20] Okada, K., Akagi, Y., *J. Chem. Eng. Japan* 1987, *20*, 11-15.

[21] Kubota, K., Hayashi, S., Inaoka, M., *J. Colloid Interface Sci.* 1983, *95*, 362-369.

[22] Lou, S.T., Ouyang, Z.Q., Zhang, Y., Li, X.J., Hu, J., Li, M.Q., Yang, F.J., *J. Vac. Sci. Technol. B Microelectron. Nanom. Struct.* 2000, *18*, 2573–2575.

[23] Guo, W., Shan, H., Guan, M., Gao, L., Liu, M., Dong, Y., *Surf. Sci.* 2012, *606*, 1462–1466.

[24] Bouwhuis, W., Van Der Veen, R.C.A., Tran, T., Keij, D.L., Winkels, K.G., Peters, I.R., Van Der Meer, D., Sun, C., Snoeijer, J.H., Lohse, D., *Phys. Rev. Lett.* 2012, *109*, 2–5.

[25] Choi, M., Na, Y., Kim, S., *Electrophoresis* 2015, *36*, 2896–2901.

[26] Meng, L., Cai, F., Zhang, Z., Niu, L., Jin, Q., Yan, F., Wu, J., Wang, Z., Zheng, H., *Biomicrofluidics* 2011, *5*, article no 044104.

[27] Berthod, A., Rodriguez, M.A., Girod, M., Armstrong, D.W., *J. Sep. Sci.* 2002, *25*, 988–995.

[28] Baroud, C.N., Gallaire, F., Dangla, R., *Lab Chip* 2010, *10*, 2032-2045.

[29] Baygentst, J.C., Saville, D.A., *J. Chem. Soc., Faraday Trans.* 1991, *87*, 1883–1898.

[30] Leroy, P., Jougnot, D., Revil, A., Lassin, A., Azaroual, M., *J. Colloid Interface Sci.* 2012, *388*, 243–256.

[31] Graciaa, A., Morel, G., Saulner, P., Lachaise, J., Schechter, R.S., *J. Colloid Interface Sci.* 1995, *172*, 131–136.

[32] Jia, W., Ren, S., Hu, B., *Int. J. Electrochem. Sci.* 2013, *8*, 5828–5837.

[33] McTaggart, H.A., *Philos. Mag.* 1922, *44*, 386–395.

[34] Beattie, J.K., Djerdjev, A.M., Warr, G.G., *Faraday Discuss.* 2009, *141*, 31-39.

[35] Vacha, R., Rick, S.W., Jungwirth, P., De Beer, A.G.F., De Aguiar, H.B., Samson, J., Roke, S., *J. Am. Chem. Soc.* 2011, *133*, 10204–10210.

[36] Renard, C., Leclercq, L., Stocco, A., Cottet, H., *J. Chromatogr. A* 2019, *1603*, 361–370.

[37] Quéré, D., *Annu. Rev. Fluid Mech.* 1999, *31*, 347–384.

[38] Bhushan, B., Pan, Y., Daniels, S., *J. Colloid Interface Sci.* 2013, *392*, 105–116.

Supporting information

Supporting information file: This Supporting information includes:

SI-1. Bubble generation reproducibility

SI-2. Required parameters for bubble generation: influence of the DMF concentration and nature of the neutral marker